Received: 22 April 2020 | Revised: 17 June 2020 | Accepted: 30 June 2020

DOI: 10.1096/fj.202000896R

RESEARCH ARTICLE

THE FASEB JOURNAL

In vivo characterization of chick embryo mesoderm by optical coherence tomography-assisted microindentation

Marica Marrese[1] | **Nelda Antonovaité**[1] | **Ben K. A. Nelemans**[2,3] | **Ariana Ahmadzada**[1] | **Davide Iannuzzi**[1] | **Theodoor H. Smit**[2,4]

[1]Department of Physics and Astronomy, Laser LaB Amsterdam, Vrije Universiteit Amsterdam, Amsterdam, The Netherlands

[2]Department of Orthopaedic Surgery, Amsterdam University Medical Centers, Amsterdam Movement Sciences, Amsterdam, The Netherlands

[3]Developmental Biology, Utrecht University, Utrecht, The Netherlands

[4]Department of Medical Biology, Amsterdam University Medical Centers, Amsterdam, The Netherlands

Correspondence
Marica Marrese, Department of Physics and Astronomy, Laser LaB Amsterdam, Vrije Universiteit Amsterdam, The Netherlands.
Email: m.marrese@vu.nl

Theodoor H. Smit, Department of Orthopaedic Surgery, Amsterdam University Medical Centers, Amsterdam Movement Sciences, Amsterdam, The Netherlands.
Email: th.smit@amsterdamumc.nl

Funding information
This work has been financially supported by the European Research Council under the European Union's Seventh Framework Programme (FP/20072013)/ ERC grant agreement no. [615170]. BN was financially supported by ZonMW-VICI grant 918.11.635 to TS.

Abstract

Embryos are growing organisms with highly heterogeneous properties in space and time. Understanding the mechanical properties is a crucial prerequisite for the investigation of morphogenesis. During the last 10 years, new techniques have been developed to evaluate the mechanical properties of biological tissues in vivo. To address this need, we employed a new instrument that, via the combination of microindentation with Optical Coherence Tomography (OCT), allows us to determine both, the spatial distribution of mechanical properties of chick embryos, and the structural changes in real-time. We report here the stiffness measurements on the live chicken embryo, from the mesenchymal tailbud to the epithelialized somites. The storage modulus of the mesoderm increases from (176 ± 18) Pa in the tail to (716 ± 117) Pa in the somitic region (mean ± SEM, n = 12). The midline has a mean storage modulus of (947 ± 111) Pa in the caudal (PSM) presomitic mesoderm (mean ± SEM, n = 12), indicating a stiff rod along the body axis, which thereby mechanically supports the surrounding tissue. The difference in stiffness between midline and presomitic mesoderm decreases as the mesoderm forms somites. This study provides an efficient method for the biomechanical characterization of soft biological tissues in vivo and shows that the mechanical properties strongly relate to different morphological features of the investigated regions.

KEYWORDS

chicken embryos, in vivo mechanical properties, microindentation, optical coherence tomography

Abbreviations: ECM, extracellular matrix; FBS, fetal bovine serum; HH, hamburger hamilton stages; LGT, low gelling temperature; MET, mesenchymal-epithelial transition; OCT, optical coherence tomography; PSM, presomitic mesoderm; SEM, standard error of the mean.

1 | INTRODUCTION

Morphogenesis is a continuous process of cell migration, tissue deformation, and growth. It is a self-organized patterning process orchestrated by the properties of the cells, which are controlled by gene expressions and chemical and physical signaling. While biochemical signals are known to play a fundamental role in the control of tissue morphogenesis,[1-4] several in vitro and in vivo studies[5-8] have shown the relevance of mechanical cues in the control of cell behavior that is central for the developmental processes. Unraveling the functional role of mechanical forces in morphogenesis is, therefore, a crucial research topic for the developmental biologists. Specifically, the processes during somite formation along the rostrocaudal axis of the embryo, such as the changing of extracellular matrix (ECM) composition, the differential migration, and the active cell contraction of epithelial cells of the mesoderm, suggest that there should be differences in mechanical properties along the rostrocaudal axis of the embryo. Mechanical forces and constraints play an important role in the embryonic development as they are able to affect the migration and differentiation of single cells.[9,10] Also, tissues and organs are influenced by mechanical forces in their cellular organization and functionalities, as shown in the tooth[11,12] and limb development.[13,14] However, the lack of methodologies enabling precise and quantitative measurements of mechanical properties of live tissues has hindered an exhaustive understanding of the role of mechanics in embryonic development. In our earlier work,[15] we proposed an experimental platform that combines micro-indentation and optical coherence tomography to assess mechanical properties in paraformaldehyde-fixed embryos. There, we have demonstrated a relationship between local mechanical properties and tissue morphology for three main embryonic regions of interest: the tail, the presomitic mesoderm, and the somitic mesoderm. While in our previous study, we reported a stiffness map averaged over two somites (S-XI and S-X) of one live embryo (Figure 8 from Marrese et al[15]), we now investigate the viscoelastic properties of the entire live chicken embryo mesoderm during somite formation. To that end, HH9-HH11 chicken embryos were cultured in filter paper sandwiches, immobilized in agarose, and indented from the ventral side along the embryo with the ferrule-top indenter, while the structure was locally imaged via optical

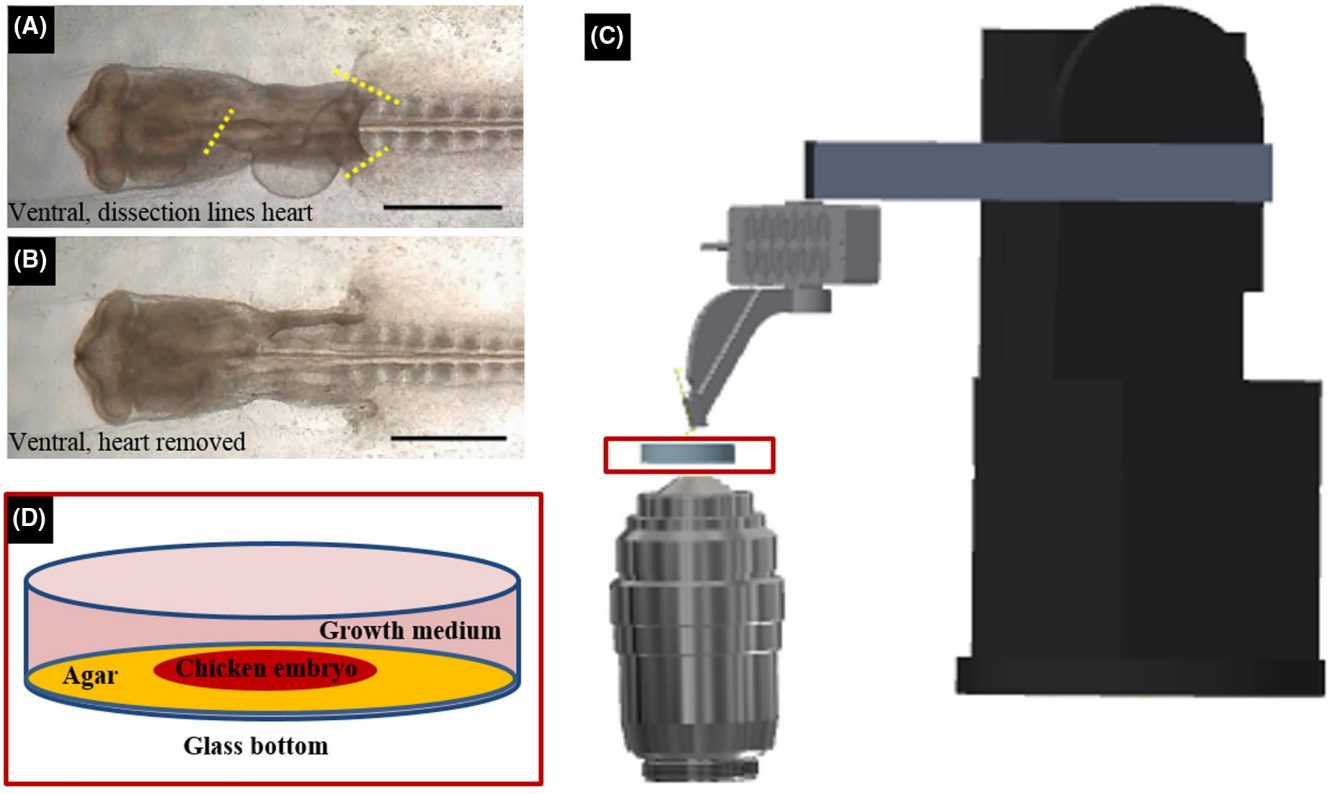

FIGURE 1 Schematic view of the setup and the sample preparation. A, Ventral view of an HH11 chicken embryo (40 hpf). Yellow lines show the dissection sites to remove the embryonic heart tube, to prevent the beating heart from disturbing the measurements. B, The same embryo as in (A), after dissection of its heart tube. Scale bar in A and B is 500 μm. C, A ferrule-top probe is equipped with an optical fiber for interferometric readout of the cantilever and with a spherical tip to indent the sample. The probe is mounted on the Z-piezoelectric actuator, which is solidly attached to an XYZ manipulator. The OCT is employed in the inverted mode. D, The embryo is embedded in agarose on its dorsal side, while the ventral side is approachable for measurements and immersed in the growth medium

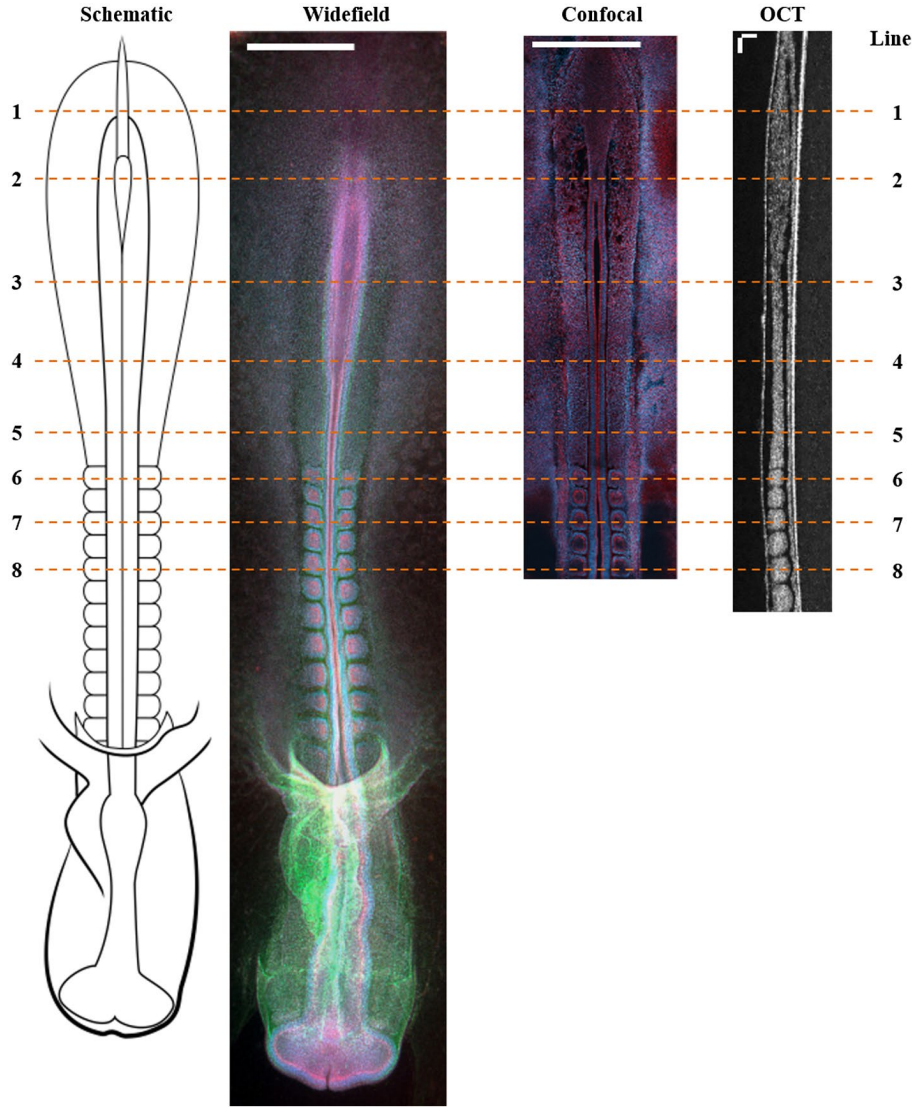

FIGURE 2 Sagittal embryo indentation points. Embryos were indented with eight transverse lines, at 10 positions with 50 μm steps, across the rostrocaudal axis, while visualized by OCT. The lines are shown imposed on a schematic embryo and a widefield immunograph. Next, there are a frontal confocal section (ventral side of the embryo) and the OCT cross-section scan (sagittal - side view) through the mesoderm. Rostral is down, and caudal is up. Immunostainings are red (actin), green (fibronectin), blue (nuclei). The scale bars are 500 μm for the widefield and confocal image and 100 μm for the OCT. The schematic view of the embryo is not to scale

coherence tomography (OCT). The simultaneous use of these two technologies allows one to perform systematic studies on two interconnected topics: on the one hand, the mechanical properties of the embryos that can be characterized through tissue microindentation; on the other hand, and the change in shape that occurs during morphogenesis. Therefore, we present a local mechanical characterization of live embryos that extends our previous work[15] by highlighting the mechanical heterogeneity and strong viscoelastic nature of the embryonic tissue in vivo. We further demonstrate that, while there are substantial differences in absolute viscoelastic responses between individual embryos, the relative trends among anatomical regions are similar and reasonably related to the maturation of the presomitic mesoderm and midline in the trunk and tail. This study opens new avenues to explore how mechanics can contribute to shaping embryonic tissues and how it affects cell behavior within developing embryos.

2 | MATERIALS AND METHODS

2.1 | Chicken embryo cultures

The embryo cultures were prepared as described somewhere else.[15] Briefly, fertilized chicken eggs, white leghorns, *Gallus gallus domesticus*,[16] were obtained from Drost BV (Loosdrecht, The Netherlands), incubated at 37.5°C in a moist atmosphere, and automatically turned every hour. After incubation for approximately 41h, HH9-HH11 chicken embryos[15,17]

were explanted using filter paper carriers[18] cultured ex ovo as modified submerged filter paper sandwiches,[19] immobilized in agarose in a 35 mm Petri dish and immersed in growth medium.[20] To avoid disturbance of the measurements by the beating of the heart that might develop, the heart tube of the ventral side of sandwiched embryos was removed (Figure 1A,B). This does not appear to inhibit further development of the spinal structures in the chick embryo. To prevent the dehydration of the live embryo during the LGT agarose curing, a droplet of the medium was carefully brought on top of the embryo, without touching the curing agarose. After approximately 3 minutes, the culture was placed in the indentation box, submerged in 25 mL of the growth medium and anatomically aligned under the OCT to precisely discriminate each indentation location.

The growth medium consisted of medium 199 GlutaMax (Invitrogen, ref. 41150-020), 10% chicken serum (GIBCO, ref. 16110-082), 5% dialyzed fetal bovine serum (FBS) (GIBCO ref. 26400-036), and 1% of a 10 000 U/mL stock solution of Penicillin/Streptomycin (GIBCO ref. 15140-122).

2.2 | Experimental setup

The setup consists of a cantilever-based indentation arm, an OCT imaging system, and a sample holder mounted on an anti-vibration table and covered with a custom acoustic isolation box to minimize mechanical noise. The setup was further equipped with a temperature control system to maintain 37°C, which was monitored at ~2 cm distance from the Petri dish with the embryo (Figure 1). The indenter is based on a micro-machined cantilever, operating as a force transducer. An extensive description and validation of the experimental setup have been reported in our previous publication.[15] The ferrule top indentation probes used in this work are fabricated in our lab, according to Refs. [21,22] and calibrated, according to Ref. [23]. Further details about the ferrule-top indenter are provided in Supplementary Figure S1. Briefly, for indentation measurements on live embryos, cantilevers with spring constant in the range of 0.34-1.2 N/m, and spheres radius between 54 and 69 μm were used. Indentations were performed in a depth-controlled mode by an oscillatory ramp profile at an indentation speed of ~0.5 μm/s, maximum indentation depth of 30 μm, and amplitude and frequency of oscillations were 0.25 μm and 2.5 Hz, respectively. Load-indentation data were used to extract storage and loss moduli,[23-25] where storage modulus corresponds to the elastic component, and loss modulus corresponds to the viscous component of mechanical response. Elasticity is the ability of materials to resist the deformation and recover to the original shape; it is commonly described in terms of softness or stiffness.

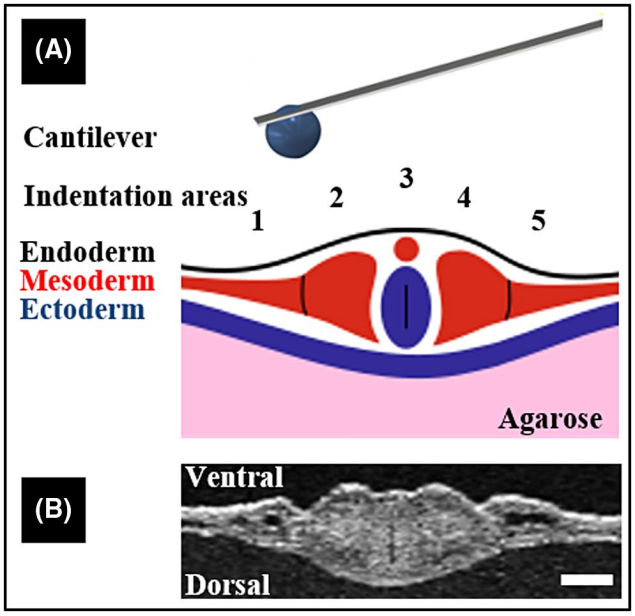

FIGURE 3 Transversal embryo indentation points. A, Schematic view and (B) OCT cross-section of the indentation positions of an HH11 embryo embedded in agarose. The scale bar is 100 μm

In contrast, viscosity describes the resistance of the material to flow and generally describes the thickness or the internal friction of a moving fluid. The ratio between loss and storage modulus is a tangent of the phase delay, $tan(\varphi)$, between oscillations in indentation and load. Tan(φ) is also called damping factor, as it describes how much energy is lost during deformation. For our experiment, storage modulus values at an averaged strain of 8 ± 1% (corresponding to an indentation depth h ~ 10-12 μm) were selected for regional comparisons, accomplishing the requirements of $h < 10\%$ of the sample thickness and small strain approximation.[26]

To find anatomical locations and follow each indentation experiment, the embryos were scanned with a spectral-domain SD-OCT (Telesto II series, Thorlabs GmbH, Germany) in inverted mode, as reported elsewhere.[15]

To perform a full mechanical characterization of the embryonic tissues, we focus on eight positions along the rostro-caudal axis of the mesoderm that show anatomical differences (Figures 2 and 3). These eight locations were indented by

TABLE 1 Anatomical regions that were indented, from caudal to rostral

Line	Anatomical region	Area
1	Tail tip	Caudal PSM
2	Caudal PSM	Caudal PSM
3	Opening neuropore	Mid PSM
4	S-IV	Rostral PSM
5	S-I	Rostral PSM
6	SI	Somitic
7	SIII	Somitic
8	SV	Somitic

TABLE 2 Anatomical regions that were indented across the embryo

Position	Somitic mesoderm		Presomitic mesoderm (PSM)		Tail	
1	**Left lateral mesoderm**	**S-LLM**	**Left lateral mesoderm**	**P-LLM**	**Left lateral mesoderm**	**/**
2	Left paraxial mesoderm	S-LPM	Left paraxial mesoderm	P-LPM	Left paraxial mesoderm	T-LPM
3	Midline	S-MD	Midline	P-MD	Midline	T-MD
4	Right paraxial mesoderm	S-RPM	Right paraxial mesoderm	P-RPM	Right paraxial mesoderm	T-RPM
5	Right lateral mesoderm	S-RLM	Right lateral mesoderm	P-RLM	Right lateral mesoderm	/

Abbreviations: LLM, left lateral mesoderm; LPM, left paraxial mesoderm; MD, midline; RLM, right lateral mesoderm; RPM, right paraxial mesoderm.

transverse lines of 10 indentations, with a step size of 50 μm (Figure 2 and Table 1). The indentation lines (500 μm length) were centered to the embryo midline so that on every rostrocaudal position, five regions of interest were measured: lateral mesoderm (regions 1 and 5), paraxial mesoderm (regions 2 and 4), and the midline (region 3) (Figure 3 and Table 2). A total of 20 embryos were explanted and examined, of which 12 embryos were used for the experiments. Other embryos were either damaged or detached during the measurements. All stiffness values are reported as mean ± SEM.

3 | RESULTS AND DISCUSSION

The indenter is based on the ferrule-top technology,[21,27] where a micro-machined cantilever, operating as a force transducer and equipped with a spherical tip, is used to determine the viscoelastic properties of the embryo via depth-controlled oscillatory ramp indentation profile.[15,24] The OCT system images the embryonic structures during the indentation measurements and allows localization of the indentation points and evaluation of the quality and the immobilization of the sample. The details of the experimental setup (Figure 1) and sample preparation are briefly reviewed in the Method section and fully reported elsewhere.[15]

Performing a full indentation map at 50 μm resolution along the embryo with the proposed depth-controlled oscillatory profile is time-consuming. A single indentation takes ~60 s, while a new somite is formed every 80 minutes; thus, it is not feasible to map the entire embryo at the same developmental stage in vivo. Therefore, to preserve the spatial accuracy along the embryo, we limited indentations to eight lines along the rostrocaudal axis of the mesoderm that are anatomically different. For further details regarding the investigated areas, we refer the reader to Figures 2 and 3.

Figure 4 shows the averaged storage modulus (E') and loss modulus (E'') of 12 in vivo HH9-HH11 chicken embryos obtained for eight positions along the rostrocaudal axis of the mesoderm. The measurements were performed at an averaged strain of ~8% and 2.5 Hz oscillation frequency. For each of the eight positions along the embryo, the plot shows the distribution of E' and E'' for five regions of interest: left and right lateral mesoderm, left and right paraxial mesoderm, and midline. From the data in Figure 4, along with OCT images, one can observe that regions with different morphologies have distinct mechanical properties. The stiffness difference between the paraxial mesoderm and the midline is more significant in the PSM and the tail than in the somitic area. In the caudal PSM, the paraxial mesoderm is very soft, while the midline stiffness E' significantly increases from (270 ± 36) to (947 ± 111) Pa (Figure 4, lines 1 to 3, mean ± SEM, $P = .0009$; .005, Wilcoxon rank-sum test; Figure S2). At the somitic levels, the midline is still the stiffest structure, but the difference with the stiffness E' of the somites is negligible (Figure 4, lines 6, 7, 8, $P = 1$, .89, .65 left side and $P = .25$, .27, .39 right side, Wilcoxon rank-sum test).

Somites III to V are slightly stiffer than somite I, but not significantly (Figure 4 lines 8 and 7 vs 6; $P = .18$, .17 left side, and $P = .66$, .07 right side, Wilcoxon rank-sum test). Similarly, the paraxial mesoderm increases its storage modulus on average from (527 ± 38) Pa in the rostral PSM up to (746 ± 44) Pa in the somitic region (Figure 4 lines 6, 7, 8 vs 4 and 5: $P = .006$, Wilcoxon rank-sum test).

Furthermore, Figure 4 shows a significant variation in stiffness E' in the caudal PSM when compared with the tail for both the midline (609 ± 63 and 270 ± 35 Pa, respectively, $P = .0002$) and the paraxial mesoderm (558 ± 44 and 181 ± 14 Pa, $P = .0001$, respectively, Wilcoxon rank-sum test).

The observed trends can be logically related to the maturation of the chicken embryo (see micrographs in Figure 2). The caudal PSM is characterized, in fact, by stem cell-like mesenchymal cells that migrate actively with large intercellular space and lack a mature extracellular matrix (ECM) (Figure 2A, confocal, and OCT section).[28] Gradually, fibronectin and laminin become more abundant and interconnect rostrally (Figure 2A widefield). This aids in anchoring the PSM cells by providing a substrate on which they can undergo collective migration and mesenchymal-epithelial transition (MET) to form epithelial spheres.[28-31] The PSM cells compact together, adhere to the ECM and each other, and become more contractile (Figure 2A confocal section, compare caudal PSM with rostral PSM),[30-32] thereby promoting fibronectin assembly.

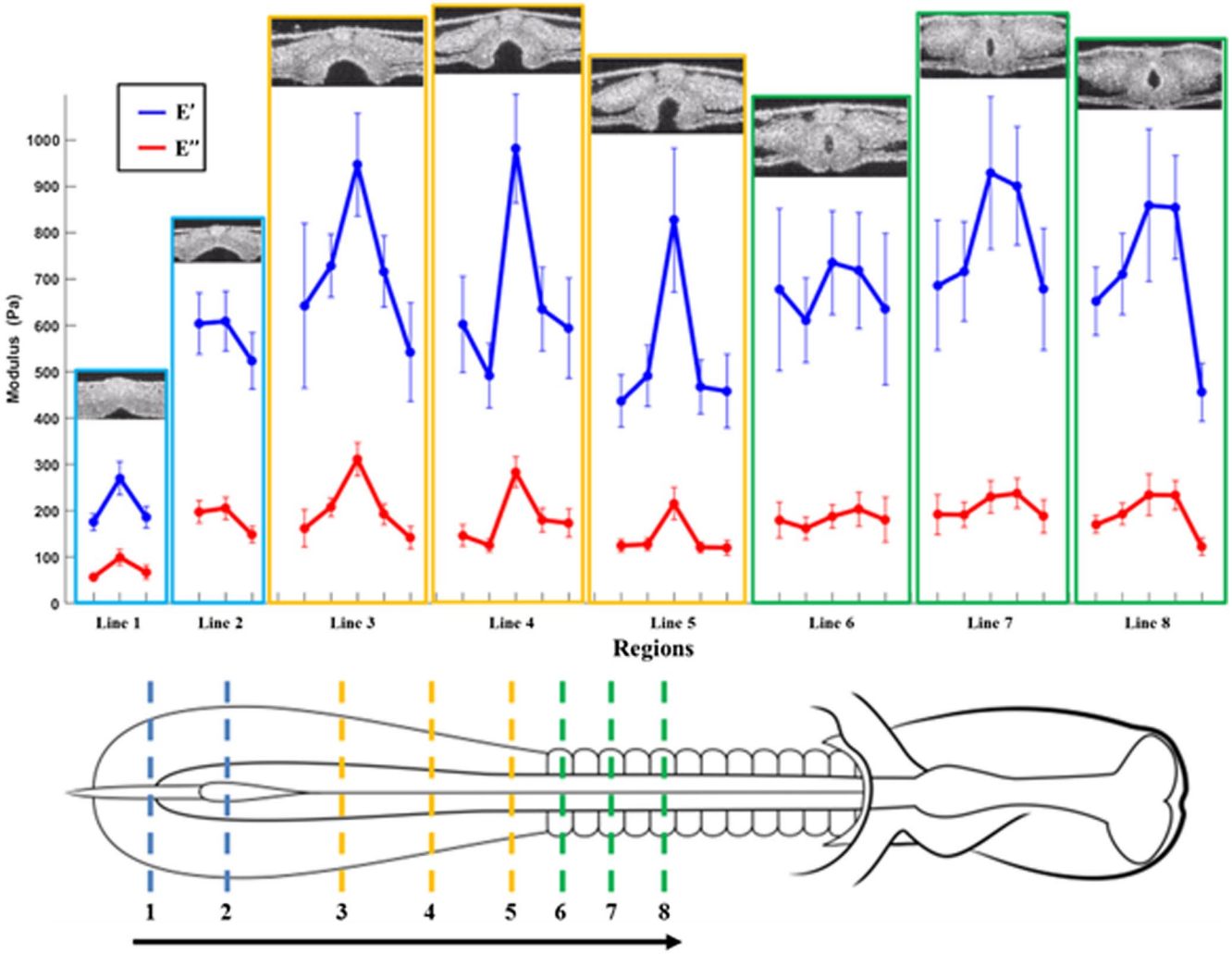

FIGURE 4 Averaged storage (E', blue) and loss (E'', red) modulus along the embryo. Transverse OCT sections show the positions of line 1 (most caudal) to line 8 (most rostral). Data points are averages of 12 embryos, with SEM error bars. Lines 1 and 2 shows three regions of interest: (1) left paraxial mesoderm, (2) midline, (3) left paraxial mesoderm. Whereas for lines 3 to 8, from left to the right, these are: (1) right lateral mesoderm, (2) right paraxial mesoderm, (3) midline, (4) left paraxial mesoderm, (5) left lateral mesoderm. The black arrow indicates the locations of the eight lines from tail to somites

Concurrently, the notochord and neural plate quickly develop a high stiffness (Figure 2, lines 8 to 6). This behavior seems to support the idea that the notochord is not only an organizer center for chemical signaling but also acts as an "embryonic spine" that plays a significant role in the mechanical integrity of the early embryo.[34] Next, the neural plate rostrally folds into the neural tube and this morphogenetic movement could be due to a stiffer tissue that undergoes neurulation (Figure 3, lines 5 and 6). This finding agrees with previous studies on the Xenopus, where morphogenetic transformations are preceded by the stiffening of the structures.[35] After neurulation, the neural tube keeps developing, but the presence of the lumen in the tube could lead to a softer tissue able to deform more when indented if compared to the compact neural groove (Figure 4, lines 4, 5 vs 6, 7, 8; Figure S3).

Dynamic indentation reveals that a viscous component is present in embryonic tissues as well (with $E' \sim 3E''$); this is illustrated by the values of loss modulus E'' in Figure 4. To describe the energy damping potential of the embryo under loading, the averaged damping factor, $tan(\varphi)$, is shown in Figure 5 as the ratio between loss and storage modulus (E''/E'). The values of $tan(\varphi)$ are comparable for the paraxial mesoderm, the midline, and the lateral mesoderm for the somitic area (P = .27-.97). However, in the tail and PSM, damping capability is higher for midline, and lower for paraxial mesoderm (P = .0001, .02; P = .02, .09, left and right, respectively, Wilcoxon rank-sum test) with the tail having overall highest damping factor ($tan(\varphi) = 0.30$-0.33 vs $tan(\varphi) = 0.26$-0.29). Specifically, this finding could be related to the status of development with the epithelial tissues (more mature and with more extracellular matrix) being more elastic and less viscous due to their nature.

It is worth to mention that averaging the viscoelasticity values from the same rostrocaudal regions over embryos

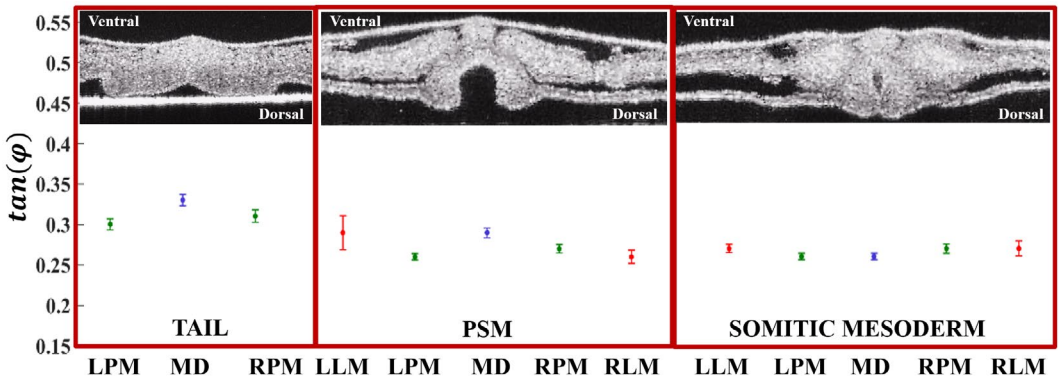

FIGURE 5 Averaged damping factor *tan*(φ) of 12 embryos over lines from the same areas: tail (lines 1 and 2), presomitic mesoderm (lines 3, 4, and 5), and somatic (lines 6, 7, and 8), and with SEM bars. Abbreviations of the region of interest from left to right: (LLM) left lateral mesoderm, (LPM) left paraxial mesoderm, (MD) midline, (RPM) right paraxial mesoderm, (RLM) right lateral mesoderm

resulted in logical trends of stiffness, that are commensurate with epithelization and matrix formation. Nevertheless, we observed substantial variation in viscoelasticity between single embryos. It appears that the biomechanical properties of the embryonic tissues may vary with age and quality of the embryo. As a point in the case, differences in the handling of the embryos could have influenced their viability and, thus, their mechanical properties. Furthermore, the indentations are influenced by the accurateness of positioning the probe tip: small variations in positioning the probe along the embryonic structures could have led to local shearing or slipping of the probe along the tissue.

It is interesting to note that some of the mechanical features observed in vivo are different from the ones described for the fixed embryo.[15] The mechanical maps reported previously for the formaldehyde-fixed embryo[15] showed an increase of stiffness along the mesoderm from the caudal tip to the rostral somites, possibly related to the effect of the formaldehyde to fix tissue by cross-linking of the biopolymers. This result is not confirmed for the live embryos, where the midline stiffness is already high in the tailbud. This finding shows the effect of formaldehyde fixation on two complex embryonic structures: the notochord and neural tube. By measuring in vivo, our instrument seems to be able to sense how the PSM (Figure 4, lines 3 and 4) is characterized by the opening of the neuropore, which has a large cell contraction as it closes to form a tube. Moreover, for the in vivo embryo, the low stiffness in the tail region is more evident if compared to the formaldehyde-fixed embryos, possibly due to the lack of structural components such as the neural tube and notochord. One can argue/state that in vivo, we are able to sense mechanical properties caused by active biomechanical processes, such as stiffening by cellular contraction, while the measurements on fixed embryo are strictly linked to tissue morphology. This behavior seems to indicate that chemical fixation has two effects on the live soft tissue: it increases tissue stiffness and reduces the damping properties of the embryonic tissues.

Comparing elasticity of the midline, the paraxial and lateral mesoderm before and after fixation, the average storage and loss moduli were found to be a factor ~2 times higher after fixation. In addition, the trends of *tan*(φ) differs from the results obtained for the paraformaldehyde-fixed embryos. Furthermore, *tan*(φ) is overall lower for the live embryo (~1.4 times). Moreover, it is interesting to mention that while observing the morphological features of the embryonic structure in vivo and after 2 hours fixation via OCT, some regions of the embryo appeared to be structurally different: the morphology of the embryo seems, in fact, more compact and dense (Figure S3). By taking a closer look at the OCT images in Figure S3 for each of the analyzed location, one can speculate that the tissue after fixation becomes denser and contains less fluid and, thus, the loss modulus increases more than storage modulus resulting in a higher *tan*(φ). These findings provide key insights into differences between in vivo and chemically treated tissue and underline the importance of using in vivo tissue to study the biomechanics of embryos.

Specifically, our measurements show that the midline already stiffens near the tail and essentially acts as an embryonic spine. The damping factor is reduced when moving from tail to head, indicating a more elastic behavior for the more mature embryonic structures. Last, the method allows for sensitive detection of structurally distinct embryonic areas, both visually and mechanically. We demonstrate that our platform can reliably measure the viscoelastic properties of the tissue with more precision than previous studies[36] and allows one to discriminate between the small embryonic structures like somites and neural tube. Our technique can be further exploited to evaluate how regional viscoelasticity triggers not only cell behavior, but also organogenesis, as already demonstrated by Mammoto et al for tooth formation,[11,12] by Damon[13,14] for limb bud organization and by Vuong-Brender and coworkers

for embryonic elongation.[37] Finally, since mechanical stress can modulate physiological processes at the cellular and tissue level, we expect that this study will support a significant step forward in gaining new insights into the relationship between altered morphogenesis, stiffness, and pathologies during embryonic development.

CONFLICT OF INTEREST

DI declares the potential conflict of interest as founder, shareholder, and advisor of Optics11.

AUTHOR CONTRIBUTIONS

TS and DI design the research; MM, NA, BN, and AA performed the experiments and analyzed the data; MM, NA, and TS wrote the manuscript. All authors critically revised the manuscript for intellectual content and approved the final manuscript.

DATA AVAILABILITY STATEMENT

All raw and processed data of this study are available from the corresponding author on reasonable request.

REFERENCES

1. Alan Mathison Turing. The chemical basis of morphogenesis. *Philos Trans R Soc Lond B Biol Sci*. 1952;237:37-72.
2. Gjorevski N, Nelson CM. The mechanics of development: models and methods for tissue morphogenesis. *Birth Defects Res C Embryo Today*. 2010;90:193-202.
3. Miller CJ, Davidson LA. The interplay between cell signalling and mechanics in developmental processes. *Nat Rev Genet*. 2013;14:733-744.
4. Pourquié O. The segmentation clock: converting embryonic time into spatial pattern. *Science (80-)*. 2003;301:328-330.
5. Discher DE, Janmey P, Wang YL. Tissue cells feel and respond to the stiffness of their substrate. *Science (80-)*. 2005;310:1139-1143.
6. Engler AJ, Sen S, Sweeney HL, Discher DE. Matrix elasticity directs stem cell lineage specification. *Cell*. 2006;126:677-689.
7. Filas BA, Xu G, Taber LA. Probing regional mechanical properties of embryonic tissue using microindentation and optical coherence tomography. In: *Methods in Molecular Biology*. Vol. 1189. Clifton, NJ; 2015:3-16.
8. Chevalier NR, Gazguez E, Dufour S, Fleury V. Measuring the micromechanical properties of embryonic tissues. *Methods*. 2016;94:120-128.
9. Lo CM, Wang HB, Dembo M, Wang YL. Cell movement is guided by the rigidity of the substrate. *Biophys J*. 2000;79:144-152.
10. Engler AJ, Sweeney HL, Discher DE, Schwarzbauer JE. Extracellular matrix elasticity directs stem cell differentiation. *J Musculoskelet Neuronal Interact*. 2007;7:335.
11. Calamari ZT, Hu JKH, Klein OD. Tissue mechanical forces and evolutionary developmental changes act through space and time to shape tooth morphology and function. *BioEssays*. 2018;40.
12. Mammoto T, Mammoto A, Torisawa Y, et al. Mechanochemical control of mesenchymal condensation and embryonic tooth organ formation. *Dev Cell*. 2011;21:758-769.
13. Damon BJ, Mezentseva NV, Kumaratilake JS, Forgacs G, Newman SA. Limb bud and flank mesoderm have distinct "physical phenotypes" that may contribute to limb budding. *Dev Biol*. 2008;321:319-330.
14. Zhu M, Tao H, Samani M, et al. Spatial mapping of tissue properties in vivo reveals a 3D stiffness gradient in the mouse limb bud. *Proc Natl Acad Sci USA*. 2020;117:4781-4791.
15. Marrese M, Antonovaite N, Nelemans BKA, Smit TH, Iannuzzi D. Micro-indentation and optical coherence tomography for the mechanical characterization of embryos: experimental setup and measurements on chicken embryos. *Acta Biomater*. 2019;97:524–534.
16. Linnaeus. *Gallus gallus subsp. domesticus*. 1758.
17. Hamburger V, Hamilton HL. A series of normal stages in the development of the chick embryo. *J Morphol*. 1951;88:49-92.
18. Chapman SC, Collignon J, Schoenwolf GC, Lumsden A. Improved method for chick whole-embryo culture using a filter paper carrier. *Dev Dyn*. 2001;220:284-289.
19. Schmitz M, Nelemans BKA, Smit TH. A submerged filter paper sandwich for long-term ex ovo time-lapse imaging of early chick embryos. *J Vis Exp*. 2016;28:e54636.
20. Palmeirim I, Henrique D, Ish-Horowicz D, Pourquié O. Avian hairy gene expression identifies a molecular clock linked to vertebrate segmentation and somitogenesis. *Cell*. 1997;91:639-648.
21. Chavan D, Gruca G, De Man S, et al. Ferrule-top atomic force microscope. *Rev Sci Instrum*. 2010;81(12):123702.
22. Chavan D, Van De Watering TC, Gruca G, et al. Ferrule-top nanoindenter: an optomechanical fiber sensor for nanoindentation. *Rev Sci Instrum*. 2012;83(11):115110.
23. Beekmans SV, Iannuzzi D. Characterizing tissue stiffness at the tip of a rigid needle using an opto-mechanical force sensor. *Biomed Microdevices*. 2016;18:1-8.
24. Antonovaite N, Beekmans SV, Hol EM, Wadman WJ, Iannuzzi D. Regional variations in stiffness in live mouse brain tissue determined by depth-controlled indentation mapping. *Sci Rep*. 2018;8:12517.
25. Van Hoorn H, Kurniawan NA, Koenderink GH, Iannuzzi D. Local dynamic mechanical analysis for heterogeneous soft matter using ferrule-top indentation. *Soft Matter*. 2016;12:3066-3073.
26. Lin DC, Shreiber DI, Dimitriadis EK, Horkay F. Spherical indentation of soft matter beyond the Hertzian regime: numerical and experimental validation of hyperelastic models. *Biomech Model Mechanobiol*. 2009;8:345-358.
27. Gruca G, de Man S, Slaman M, Rector JH, Iannuzzi D. Ferrule-top micromachined devices: design, fabrication, performance. *Meas Sci Technol*. 2010;21:094033.
28. Bénazéraf B, Francois P, Baker RE, Denans N, Little CD, Pourquié O. A random cell motility gradient downstream of FGF controls elongation of an amniote embryo. *Nature*. 2010;466:248-252.
29. Cheney CM, Lash JW. An increase in cell-cell adhesion in the chick segmental plate results in a meristic pattern. *J Embryol Exp Morphol*. 1984;79:1-10.
30. Oster GF, Murray JD, Harris AK. Mechanical aspects of mesenchymal morphogenesis. *Development*. 78; 1983;83-125.
31. Sato Y, Nagatoshi K, Hamano A, et al. Basal filopodia and vascular mechanical stress organize fibronectin into pillars bridging the mesoderm-endoderm gap. *Development*. 2017;144:281-291.

32. Goto Y. A 2-dimensional mechanical model of the formation of a somite. *Int J Numer Anal Model*. 2013;10:203-220.
33. Bard JBL. A traction-based mechanism for somitogenesis in the chick. *Roux's Arch Dev Biol*. 1988;197:513-517.
34. Corallo D, Trapani V, Bonaldo P. The notochord: structure and functions. *Cell Mol Life Sci*. 2015;72:2989-3008.
35. Zhou J, Kim HY, Davidson LA. Actomyosin stiffens the vertebrate embryo during crucial stages of elongation and neural tube closure. *Development*. 2009;136:677-688.
36. Agero U, Glazier JA, Hosek M. Bulk elastic properties of chicken embryos during somitogenesis. *Biomed Eng Online*. 2010;9:19.
37. Vuong-Brender TTK, Ben Amar M, Pontabry J, Labouesse M. The interplay of stiffness and force anisotropies drives embryo elongation. *eLife*. 2017;6:1–49.

SUPPORTING INFORMATION

Additional Supporting Information may be found online in the Supporting Information section.

How to cite this article: Marrese M, Antonovaité N, Nelemans BKA, Ahmadzada A, Iannuzzi D, Smit TH. In vivo characterization of chick embryo mesoderm by optical coherence tomography-assisted microindentation. *The FASEB Journal*. 2020;34:12269–12277. https://doi.org/10.1096/fj.202000896R